

The pre-hydrolysis state of p21^{ras} in complex with GTP: new insights into the role of water molecules in the GTP hydrolysis reaction of ras-like proteins

Axel J Scheidig*, Christoph Burmester and Roger S Goody*

Background: In numerous biological events the hydrolysis of guanine triphosphate (GTP) is a trigger to switch from the active to the inactive protein form. In spite of the availability of several high-resolution crystal structures, the details of the mechanism of nucleotide hydrolysis by GTPases are still unclear. This is partly because the structures of the proteins in their active states had to be determined in the presence of non-hydrolyzable GTP analogues (e.g. GppNHp). Knowledge of the structure of the true Michaelis complex might provide additional insights into the intrinsic protein hydrolysis mechanism of GTP and related nucleotides.

Results: The structure of the complex formed between p21^{ras} and GTP has been determined by X-ray diffraction at 1.6 Å using a combination of photolysis of an inactive GTP precursor (caged GTP) and rapid freezing (100K). The structure of this complex differs from that of p21^{ras}-GppNHp (determined at 277K) with respect to the degree of order and conformation of the catalytic loop (loop 4 of the switch II region) and the positioning of water molecules around the γ -phosphate group. The changes in the arrangement of water molecules were induced by the cryo-temperature technique.

Conclusions: The results shed light on the function of Gln61 in the intrinsic GTP hydrolysis reaction. Furthermore, the possibility of a proton shuffling mechanism between two attacking water molecules and an oxygen of the γ -phosphate group can be proposed for the basal GTPase mechanism, but arguments are presented that render this protonation mechanism unlikely for the GTPase activating protein (GAP)-activated GTPase.

Introduction

Guanine–nucleotide binding proteins are involved in a broad range of intracellular processes involving signal transduction (small p21^{ras}-like proteins, heterotrimeric G proteins), vesicular transport (Rab proteins) and polypeptide synthesis (elongation and initiation factors) (for reviews, see [1–3]). Their properties are strongly coupled to the state of the bound nucleotide, in general being active and interacting with effector proteins if guanine triphosphate (GTP) is bound and inactive if guanine diphosphate (GDP) is bound [1]. GTP hydrolysis to GDP is performed intrinsically or in a dramatically enhanced manner upon interaction with GTPase-activating proteins (GAPs) [4]. The mechanism of GTP hydrolysis and the associated rearrangements in protein topology are central to the function of these proteins. Elucidation of the chemical mechanism of the bond cleavage between the β -phosphate and γ -phosphate has been the focus of numerous studies involving isotope labelling [5], site-directed mutagenesis [6,7], X-ray diffraction [8,9], NMR spectroscopy [10,11] and molecular dynamic simulations [12,13]. Much of the experimental data is most easily interpreted in terms of an associative mechanism with an activated water molecule acting as a

nucleophile performing an in-line S_N2-like attack on the phosphorus atom followed by cleavage of the bond between the β - and γ -phosphates. The absence of an obvious candidate for a general base that abstracts a proton from the attacking water molecule, together with evidence favouring a dissociative mechanism in the non-enzymatic hydrolysis of GTP, has led to the suggestion that a dissociative type of mechanism should be considered. Recently the γ -phosphate group itself has been suggested to be the base responsible for deprotonation of the hydrolysing water molecule in a substrate-assisted catalysis mechanism [14] producing an attacking hydroxy-ion. The possible involvement of other water molecules was not discussed.

Much of the evidence on the mechanism of GTP hydrolysis by p21^{ras} and related GTPases comes from the structure of such proteins with non-hydrolysable GTP analogues (GppNHp, GTP(γ -S) or GppCH₂p) at the active site. It is not clear, however, whether these structures can be used for detailed mechanistic interpretations. In the ATPase field there is reported evidence (e.g. for the chaperone DnaK) that AppNHp does not properly mimic the ATP. In past work, we used a photosensitive

Address: Max-Planck Institute for Molecular Physiology, Abteilung für Physikalische Biochemie, Otto-Hahn-Straße 11, 44227 Dortmund, Germany.

*Corresponding authors.

E-mail: scheidig@mpi-dortmund.mpg.de
goody@mpi-dortmund.mpg.de

Key words: crystal structure, freeze-trapping, GTP-binding protein, hydrolysis mechanism, reaction intermediate

Received: 1 April 1999

Revisions requested: 18 May 1999

Revisions received: 16 June 1999

Accepted: 21 July 1999

Published: 25 October 1999

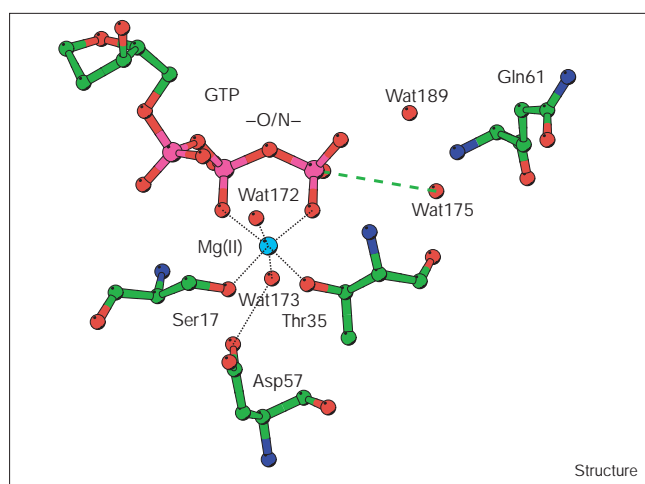
Structure November 1999, 7:1311–1324

0969-2126/99/\$ – see front matter

© 1999 Elsevier Science Ltd. All rights reserved.

precursor of GTP (caged GTP) at the active site of p21^{ras} to allow crystallisation of this complex and generation of the genuine substrate, GTP, at the active site [15]. In combination with the Laue method for X-ray diffraction at a synchrotron source, this allowed determination of the structure of the p21^{ras}-GTP complex, as well as that of p21^{ras}-GDP after enzymatic hydrolysis had occurred in the crystal. Although these experiments were technically successful, limitations of crystal quality and the Laue diffraction method used in these resulted in only moderate resolution in the electron-density map so that several regions of the protein were not well defined, and subsequent improvement of crystal quality for monochromatic diffraction led to only a modest improvement in this respect under Laue conditions [16]. Thus, questions such as what is the definition of the conformation of the switch II region of the protein, which is involved in catalysis? and what are the positions of water molecules potentially involved in catalysis? could not be addressed in the genuine GTP state, but only in the better resolved GppNHp state. Figure 1 summarises the remaining open questions that were the focus of the work presented here. The structure of Rap2a, a member of the Ras superfamily, with GTP at the active site has been published recently [17]. This is an uncharacteristically slow GTPase, however, and the structural model obtained also lacks water molecules at the active site.

Figure 1



The active site of p21^{ras} in complex with GTP and the catalytic mechanism for the intrinsic hydrolysis. The residues and atoms involved in indirect or direct participation in the intrinsic GTP hydrolysis reaction are illustrated and give rise to the following questions. If GTP serves as the general base that is protonated during the reaction, how does the proton from the attacking water get there? A glutamine or glutamic acid at position 61 is necessary for the intrinsic reaction [7] – what is its function? In some crystal structures of p21^{ras}-GDP, water molecule Wat173 is not visible – is it directly involved in the hydrolysis reaction? Most structures have been solved with GppNHp – is it a good analogue for GTP? This figure was generated using the program Bobscrip [59].

Here we report on the combination of photolysis of caged GTP in crystals of p21^{ras} with rapid freezing to trap the transiently formed GTP state, leading to a high resolution p21^{ras}-GTP structure. A comparison of the p21^{ras}-GTP structure with that of the structure of a model for the transition state of the GAP-activated p21^{ras} GTPase arising from other work allows a detailed mechanistic description of the approach to the transition state from the ground state. In addition we have re-determined the p21^{ras}-GppNHp structure at the two commonly used temperatures, 100K and 277K. The comparison of the 100K and 277K structures reveals a significant shift in the positions of mechanistically important water molecules.

Results

Production of p21^{ras}-GTP and p21^{ras}-GDP crystals

We have shown previously [18] that the use of the pure *R*-1-(2-nitrophenyl)ethyl GTP ester diastereoisomer rather than the mixed *RS*-isomers or the pure *S*-caged isomer gave crystals of the complex that diffracted to much higher resolution. The protecting group can be removed by irradiation of the sample with light in the wavelength range 300–360 nm [19]. In principal, several different light sources can be used for photolysis. Depending on the conditions of the experiment, however, the energy load per unit time must be optimised to avoid damage to the sample although achieving essentially complete conversion to the natural substrate or ligand (for a more detailed discussion see [20]). Best results for the present purpose were obtained with a 100 W mercury lamp in continuous mode using the characteristic line at 313 nm (see the Materials and methods section).

Crystals of p21^{ras}-GTP frozen rapidly in liquid nitrogen approximately two minutes after photolysis of caged GTP diffracted as strongly as crystals of unphotolyzed p21^{ras}-caged GTP of comparable size. Photolysis and removal of the cage group, therefore, followed by subsequent reaction of the reactive photolysis product nitrosoacetophenone with dithiothreitol (DTT) caused no detectable crystal damage. We could never observe any electron density in the crystals that can be related to either DTT or reaction products with nitrosoacetophenone. Mass spectrometry did not indicate any covalent modification of the protein (data not shown, see the Materials and methods section). Crystals of p21^{ras} complexed with GDP arising from GTP hydrolysis after photolysis showed significantly reduced diffraction quality compared with those of p21^{ras}-GTP. Given that the p21^{ras}-GDP crystals were derived from p21^{ras}-GTP, it is apparent that the reduction in crystal quality was not caused by the irradiation protocol but by events accompanying GTP hydrolysis.

Comparison of p21^{ras}-GTP and p21^{ras}-GppNHp

There are no differences in the general fold of the protein and in the mainchain and sidechain positions of most of the residues between the two structures. Comparing the

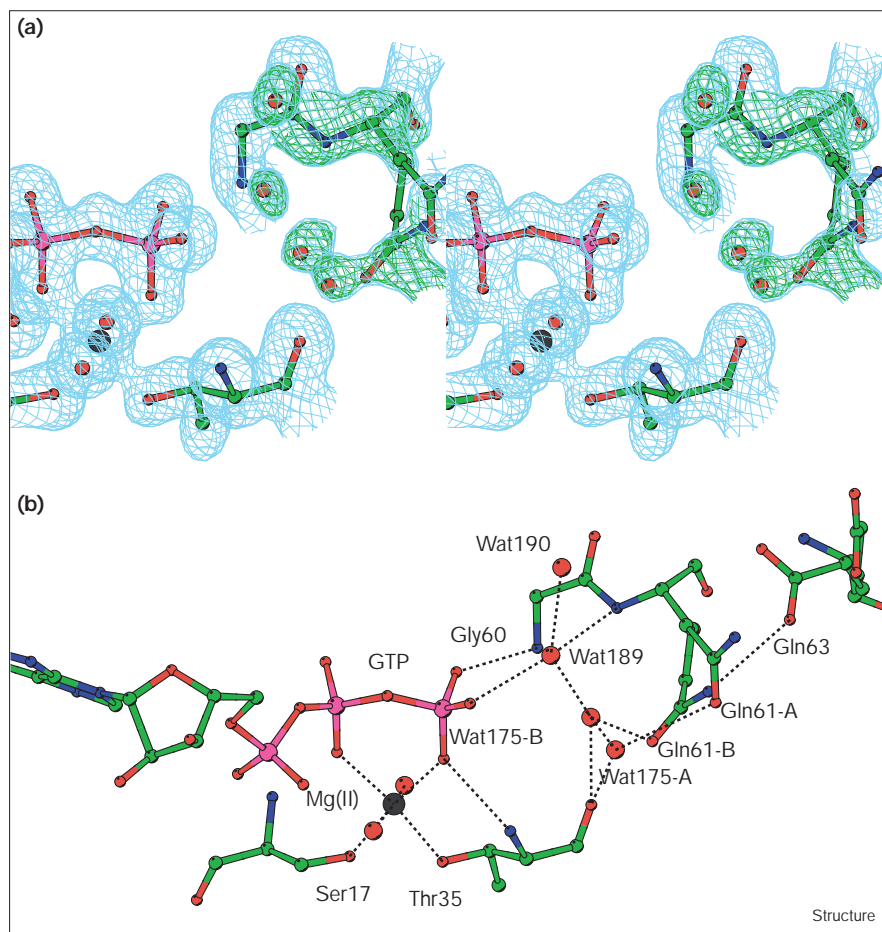
100K structure of p21^{ras}-GTP with the 277K structure of p21^{ras}-GppNHp (PDB entry 5P21 [8]) we observed significant differences in three protein regions, namely residues 30–31, 61–68 and 107–108. Furthermore, most of the water molecules were shifted, in particular the three water molecules nearest the γ -phosphate group. These structural changes could be a consequence of the different nucleotide bound at the active site or could be caused by the change in temperature for data collection. To be able to distinguish between these possibilities we re-determined the crystal structure of p21^{ras}-GppNHp at 100K and included it in the comparison. (The temperature used for data collection is given in parentheses after the structure name, for example p21^{ras}-GppNHp (277K) refers to the PDB entry 5P21 [8]. Water molecules that occupy the same position as in p21^{ras}-GppNHp (277K) within a sphere radius of 0.5 Å or are shifted equivalently have the same number as in p21^{ras}-GppNHp (277K). New numbers are assigned to all other water molecules.)

For residues 107–108, different conformations were already observed and discussed [18] and appear not to be related to the active site situation. The difference in the peptide bond orientation between residues Asp30 and Glu31 reflects an alternative orientation for the peptide bond oxygen of Asp30. The different position of Asp30-O is of interest because in this orientation there is a hydrogen bond between Asp30-O and the 3' hydroxy group of the ribose ring of GTP ($d(\text{Asp30-O-GTP-O3'}) = 3.48 \text{ \AA}$). In the structure of p21^{ras}-GTP (100K) this orientation has a significantly higher occupancy compared with the major orientation in the complex with GppNHp (p21^{ras}-GppNHp (277K) [8] and p21(G12P)^{ras}-GppNHp (277K) [21]). The minor orientation was used for the hydrogen-bond network figure in [8]. This hydrogen bond appears to be weak, as evidenced by the fact that it is not 100% formed in the structure and the fact that 3'-modified GTP and GDP analogues bind with high affinity to p21^{ras} [22].

The largest deviations between the structures of p21^{ras}-GTP (100K) and p21^{ras}-GppNHp (277K) are observed around the so-called catalytic loop of the switch II region. This loop (residues 60–64) and the start of helix $\alpha 2$ (residues 65–67) are the most poorly defined regions in the whole protein, as reflected by the B-factor plot [8]. In both 100K structures (p21^{ras}-GTP and p21^{ras}-GppNHp), however, the amino acids from Gln61 to Met67 are much better defined than in the 277K structures, both with respect to the mainchain and, with the exception of Glu62, with respect to the sidechains as well. In three independently solved structures of p21^{ras}-GTP (see the Materials and methods section), we observed essentially the same electron-density distribution for the mainchain and sidechains. In the case of Gln61 and Glu63, however, two slightly different alternative sidechain conformations have to be discussed for p21^{ras}-GTP (100K) but not for

p21^{ras}-GppNHp (100K). The two alternative conformations for the sidechain orientation of Gln61 are approximately equally occupied. The interpretation of the observed electron density as two conformations of Gln61 and not as statistically disordered water molecules is on the basis of the very good definition of two water molecules (Wat175-A and Wat175-B) near the γ -phosphate group (Figure 2). Because of steric overlap it is not possible to have both water molecules (Wat175-A and Wat175-B) simultaneously in these two positions ($d = 1.6 \text{ \AA}$). The refinement in the program SHELXL [23] as two alternative water molecules gave an occupancy of 60% for Wat175-A (B factor = 29 \AA^2) and of 40% for Wat175-B (B factor = 27 \AA^2). In all three independently refined p21^{ras}-GTP structures positive difference electron density in simulated annealing omit maps could be observed for these two water positions as well as density reaching from the C α backbone at position 61 towards the position of Wat175-A. The correlation coefficients of the simulated annealing omit maps for the three individually refined data sets was between 0.93 and 0.95 (omitting all atoms within a sphere of 7 Å diameter around water position Wat175-A for refinement and calculating the map for a sphere of 4 Å diameter around that position). Placing the sidechain of Gln61 in other conformations resulted in strong negative difference electron density for these orientations. On the basis of these observations we refined the Gln61 sidechain in two alternative conformations that could form hydrogen bonds to either one of the two water molecules Wat175-A and Wat175-B (Figure 2b). A similar orientation for Gln61 was proposed (but not observed directly) as the 'catalytically active conformation' in p21^{ras}-GppNHp [8] in which Gln61 was proposed to serve as a base (with the help of Glu63) to activate the attacking water molecule [8]. In all three independent structures we never observed an orientation of the Gln61 sidechain in direct contact with the γ -phosphate group. Another major difference in the interpretation of this loop region occurs for the sidechain orientation of residues Glu63, Tyr64 and Met67 (Figure 3). As a consequence of the two alternative conformations for Gln61, the orientation of Glu63 can also be interpreted with two similar conformations, each making a hydrogen bond between the sidechain atoms Gln61-NE2 and Glu63-OE1 (Figure 2b). The two alternative water positions and the conformations of Gln61 and Glu63 were initially refined independently, however, because they refined with nearly the same occupancies in later refinement steps they were treated as an ensemble giving for all three parts the same occupancy. The whole of residue Tyr64 is very well defined and occupies the space in which originally the sidechain of Glu63 was modelled in the 277K GppNHp structures. Close to the position of Tyr64 in the 277K GppNHp structure the sidechain of Met67 is now positioned in very well-shaped electron density. Because the electron density for this loop region compared with the rest of the protein is weak we questioned whether these new conformations are really supported by the data. We have

Figure 2



Stereo representation of the active site of p21^{ras} in complex with GTP. Displayed are the γ -phosphate and β -phosphate of the nucleotide, the Mg^{2+} cation with its coordinating water molecules Wat172 and Wat173, the amino acid residues Ser17, Thr35, Gly60 and Gln61 (conformation A and B) together with the water molecules around the γ -phosphate group. The figure shows the active site viewed onto the plane formed by the β , γ -bridging heteroatom and the γ -phosphorus and β -phosphorus.

(a) Superposition of the $F_o - F_c$ (cut-off 1σ in green) and $2F_o - F_c$ σA -weighted (cut-off 2σ in blue) electron-density maps calculated after simulated annealing refinement (merged data set T1 + T2 + T3) omitting the water molecules Wat175, Wat189, Wat190 and the amino acid residues 61 and 63, respectively. (b) The observed and discussed interactions based on the interpretation of the electron-density distribution. Hydrogen bonds are shown as dashed lines. This figure was generated using Bobscript [59].

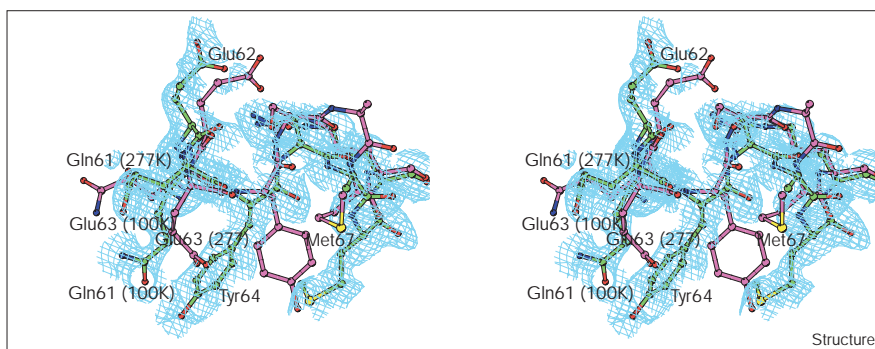
therefore generated 500 different low-energy conformations (mainchain and sidechain rotamers) for the whole loop region from residues 60–68 (conformations generated with the program ICM 2.7 [24]) and performed refinement with the program CNS [25]. Evaluation of the different conformations was performed by simulated annealing refinement of the individual conformations and monitoring the R_{work} and R_{free} residual factors, respectively. Interpretation of simulated annealing omit maps for the refined conformations clearly selected the same conformations for residues Gln61, Glu63, Tyr64 and Met67 as originally interpreted from the electron-density map (Figure 3). This structural interpretation (including two correlated, alternative conformations for Gln61 and Glu63) refined 1.5% lower in the R_{free} value compared with the GppNHp (277K) conformation. This different interpretation for the positioning of the sidechains is most probably because of the better, however still weakly defined, electron-density distribution in this region for the 100K structures. Using this loop structure for a re-refinement of p21(G12P)–GppNHp [21] including cross-validation (R_{free} test) resulted in a drop of $\sim 0.7\%$ for both R_{work} and R_{test} (data not shown).

Comparison of p21^{ras}–GTP and p21^{ras}–GDP

The main differences in the two nucleotide-bound states are within the switch I and switch II regions, as already observed and discussed (for a review see [2]). The quality of the electron-density map in these two loop regions in the GDP structure derived from p21^{ras}–GTP by hydrolysis in the crystal is very poor and might reflect an ensemble of different conformations. This disorder is most probably the result of lost interactions of protein atoms with the γ -phosphate group (in particular, Thr35 and Gly60 are no longer anchored). In addition to the uncertainty in positioning of these two loop regions, the N-terminal part of helix $\alpha 2$ (residues 65–71) refines with very high B factors for mainchain and sidechain atoms and the electron-density is not well defined, possibly indicating a tendency towards reorientation of this helix. Given that the switch I and the switch II regions are part of the same crystal-packing interface related by the twofold axis, changes in this region could be the cause of the observed shortening of the longest cell axis from ~ 159 Å to ~ 154 Å, which is directly connected to the progress of the hydrolysis of GTP to GDP in the crystal. Furthermore, rearrangements

Figure 3

Stereo representation of part of the loop L4 of the switch II region of p21^{ras}-GTP (100K). The $2F_o - F_c$ σ A-weighted electron-density map contoured at 1.5σ superimposed with the residues 61–68. In green, the residues Gln61 (only alternative conformation A), Glu62, Glu63 (only alternative conformations A), Tyr64, Ser65, Ala66, Met76 and Arg68 of p21^{ras}-GTP (100K) are superimposed with the corresponding residues of p21^{ras}-GppNHp (277K) in magenta (PDB entry 5P21 [8]). This figure was generated using Bobscript [59].



of these loops can cause a break in crystal symmetry and perhaps even a kind of twinning; these aspects are currently being analysed. The coordination sphere of the divalent cation Mg^{2+} is well defined and will be discussed because it is relevant to the mechanism. The position of Thr35-OG1 in the p21^{ras}-GTP structure is replaced by a new water molecule and because of this and the loss of the γ -phosphate group, which is also replaced by a water molecule, the octahedral coordination sphere of Mg^{2+} becomes slightly distorted. In contrast to the interpretation of low-resolution p21^{ras}-GDP structures [16,26] and in agreement with PDB entry 4Q21 [27] we observe electron density, albeit weak, for a water molecule between the sidechain atom Asp57-OD1 and the Mg^{2+} ion, indicating no loss of this water molecule during the hydrolysis reaction (Wat173 in the p21^{ras}-GppNHp structures).

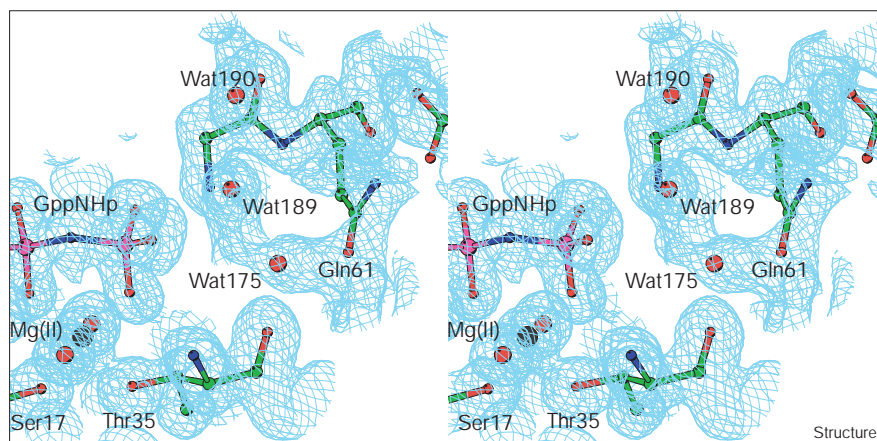
The γ -phosphate environment and temperature dependency of the associated water structure

For the discussion of the hydrolysis mechanism we describe and compare the structural environment around the γ -phosphate of GTP with the stereo-chemical situation and water arrangement seen in the high resolution crystal structures of p21^{ras} in complex with GppNHp [8,21]. Because the p21^{ras}-GTP structures were determined at 100K after shock-freezing the crystal in liquid nitrogen (no addition of cryo-protectant was needed), we have ‘re-determined’ the p21^{ras}-GppNHp structure using the same crystallisation and freezing conditions as for p21^{ras}-GTP. The different structures were refined in parallel using identical refinement strategies (see the Materials and methods section). In the p21^{ras}-GppNHp (277K) complexes, three water molecules, Wat172, Wat173 and Wat175, are well conserved in position and refine with below-average temperature factors (Figure 4). In all crystal structures of GTP-binding proteins a similar water structure around the γ -phosphate was observed when GppNHp or GTP γ S was bound (elongation factor (EF)-Tu-GppNHp [28,29]; $G_i\alpha$ -GTP γ S [30]). The water molecules Wat172 and Wat173 are part of the Mg^{2+} coordination sphere and Wat175 is positioned approximately in-line with the scissile

β,γ -P-O bond. On the basis of its position, water molecule Wat175 was proposed to be involved in an S_N2 -like in-line attack on the γ -phosphate group [8].

A striking difference between the p21^{ras}-GppNHp (277K) structures and the p21^{ras}-GTP (100K) structure presented is the exact positioning of water molecule Wat175 and two additional water molecules that are within a 6 Å radius of the γ -phosphate group. In the GTP structure there is no electron density visible at the position occupied by water molecule Wat175 in the GppNHp (277K) structures. The next closest water in the p21^{ras}-GTP (100K) structure to this position is 0.8 Å further away from the γ -phosphate and in hydrogen-bonding distance to the carbonyl group of Gln61 (Figures 2,5,6). The shape of the electron density of this water molecule is unusual. It is not spherical as for the well-defined water molecules of the Mg^{2+} coordination sphere, but has a pear-like shape with the smaller end oriented towards the position occupied by Wat175 in the GppNHp (277K) complexes. This feature was seen in all three independently refined structures of p21^{ras}-GTP (100K) and therefore cannot be explained by random noise. Furthermore, we observe an elongated electron density close to the positions of the GppNHp (277K) waters Wat189 and Wat190. Interpretation of this electron density as two water molecules (GTP-Wat189 and GTP-Wat190) and refining their positions placed them ~ 0.9 – 1.3 Å apart from the corresponding GppNHp (277K) water molecules shifted in direction towards the γ -phosphate group. These four water molecules (Wat189 and Wat190 of GppNHp (277K) and of GTP (100K), respectively) are lined up in a manner that has the appearance of a water channel coming from the surface of the protein reaching to the γ -phosphate (Figure 5a). The same shift for these three water molecules is observed comparing p21^{ras}-GppNHp (100K) with p21^{ras}-GppNHp (277K) (Figure 5b). The only difference between p21^{ras}-GTP (100K) and p21^{ras}-GppNHp (100K) in this region is that we do not observe two alternative positions for the shifted water molecule Wat175 as seen for GTP-Wat175 but the same pear-like shape of the electron density extending from this water molecule making a

Figure 4



Stereo representation of the $2F_o - F_c$ σ_A -weighted (cut-off 2σ in blue) electron-density distribution at the active site of p21^{ras} in complex with GppNHp observed at 100K. Displayed are the γ -phosphate and β -phosphate of the nucleotide, the Mg^{2+} cation with its coordinating water molecules Wat172 and Wat173, the amino acid residues Ser17, Thr35, Gly60 and Gln61 together with the water molecules Wat175, Wat189 and Wat190 around the γ -phosphate group. The view is onto the plane formed by the β , γ -bridging heteroatom and the γ -phosphorus and β -phosphorus. This figure was generated using Bobscript [59].

'bridge' to water molecule Wat189 (Figure 4). The structure determination at two different temperatures therefore enabled us to distinguish between structural differences caused by the different nucleotide bound in the active site of p21^{ras} and the two different temperatures used for data collection, respectively.

Discussion

Rearrangement from the GTP- to the GDP-bound state

The simplest description of the change in structure of the effector loop is that on GTP hydrolysis, the well defined single conformation is lost and replaced by a complex mixture of individual conformations. The main reason for this is the loss of interactions of the highly conserved Thr35 with the γ -phosphate group through its mainchain NH and with the attacking water molecule through its mainchain carbonyl group (Figure 6). The sidechain hydroxyl of this residue is also a ligand of the Mg^{2+} ion in the GTP state, but this interaction is also lost on GTP hydrolysis. The loss of these interactions allows Thr35 and its neighbouring residues to move away from the nucleotide. The largest resulting change is in Tyr32, as documented previously. The loss of specific structure of the effector loop is in harmony with recent results on the kinetics of the interaction of Ras with its effector Raf [31], where it was shown that the association process between these two proteins is dramatically decreased in rate in the GDP state, which can be interpreted as arising from the entropic disadvantage of the existence of a large number of possible structures in this region.

In the terminology of GTP-binding proteins, loop L4 is called the 'catalytic loop', reflecting the fact that its residues were recognized to be actively involved in the hydrolysis reaction. This loop is part of the switch II region, which is proposed to reorientate upon or after GTP hydrolysis (for a detailed discussion see [30,32]). The observed low quality of the electron density in this region

and the high B factors for these residues in all p21^{ras}-GDP structures might be a result of the tendency of helix $\alpha 2$ to partially unwind and reorientate on hydrolysis of GTP. In the crystal form of p21^{ras} used (residues 1–166 of p21^{ras}), however, the extent of reorientation for this helix is limited because larger movements would destroy major crystal-packing interactions [18]. Upon hydrolysis we observe significant shrinkage of the long cell axis (c) from ~ 159 Å to ~ 154 Å, which is a further indication for modifications in this crystal-packing interface. For the discussion of the hydrolysis reaction mechanism, these reorientations seem to be unimportant (the GTP hydrolysis reaction occurs at almost the same rate in the crystal as in solution [15]) because it is an adjustment to the new situation in the nucleotide-binding site that occurs after removal of the cleaved inorganic phosphate. Local conformational changes in these two regions as a result of the adaptation of the protein to the new nucleotide state (loss of the γ -phosphate group) probably cause crystal lattice disorder and consequently loss of diffraction quality.

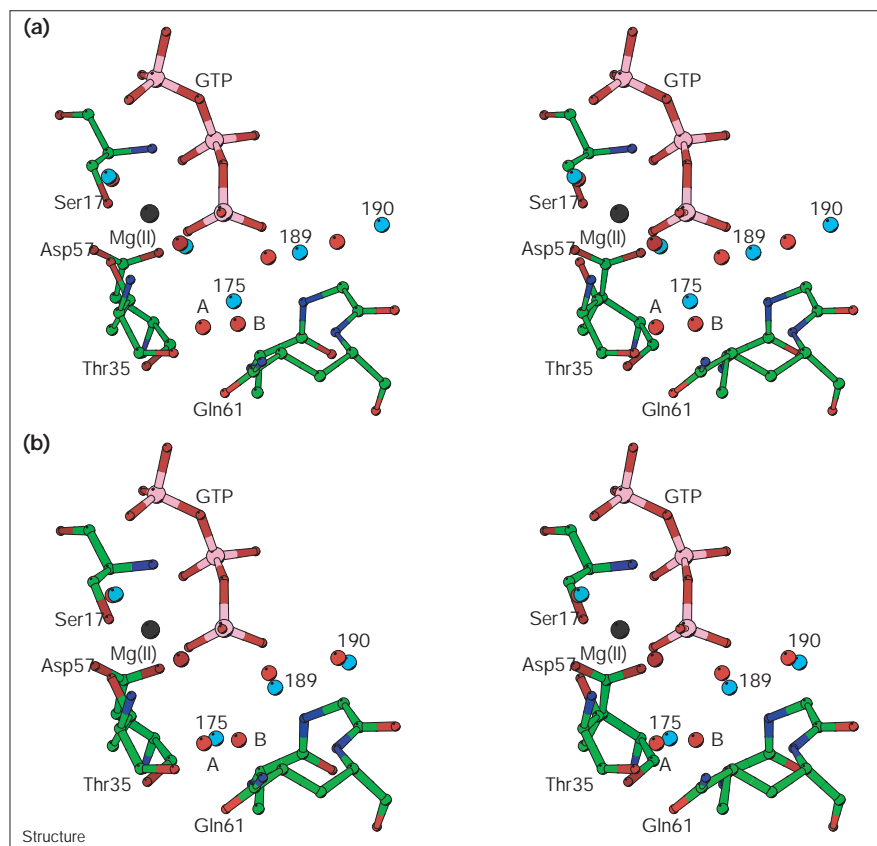
The results obtained in the present work show clearly that the water molecule between Asp57 and the Mg^{2+} ion is not lost upon GTP hydrolysis. We therefore assume that the earlier conclusion that this water molecule is lost was the result of poor electron density caused by low resolution and crystal damage.

Temperature-induced shift of water positions

The exact positioning of water molecules is crucial for almost all reactions of biomacromolecules. For the exact determination of most water molecule positions, however, high-resolution X-ray diffraction data of high quality are required. In recent years the technology of cryocrystallography [33,34] has allowed the high-resolution structure determination of biomacromolecules that could not have been solved under conventional conditions (~ 277 K). There

Figure 5

Stereo representation of the active site around the γ -phosphate group without electron density. The wall eye stereo pictures show the active site viewed along the bond between the non-ligated ^3O and the γ -phosphorus. Displayed are the triphosphate chain of GTP, the Mg^{2+} cation, water molecules Wat175 (alternative positions A and B of p21^{ras}-GTP), Wat189 and Wat190 and residues Lys16, Ser17, Thr35, Gly60 and Gln61 (conformation A). The water molecules of p21^{ras}-GTP are displayed as red spheres and those of p21^{ras}-GppNHp as cyan spheres. Comparison of the p21^{ras}-GTP structure determined at 100K with (a) the p21^{ras}-GppNHp structure determined at 277K (PDB entry 5P21 [8]) and (b) the structure determined at 100K (this work). This figure was generated using Bobscript [59].



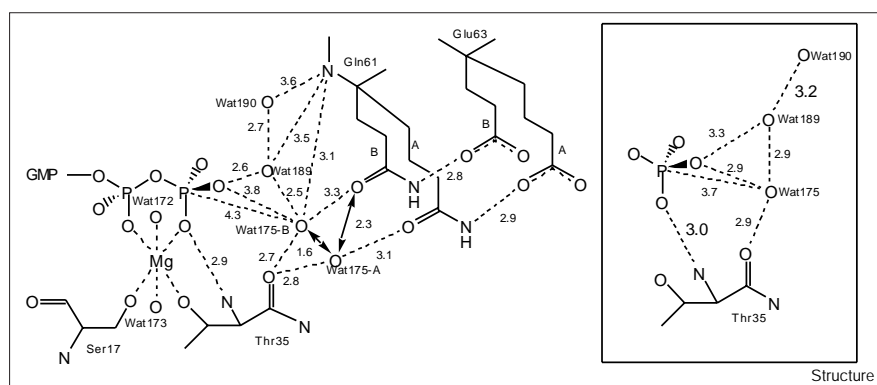
is, however, no reported example of a study of the positioning of water molecules as a function of temperature. In the present work, we observed a significant shift in the position of 15 out of 212 water molecules when we compared the p21^{ras}-GTP structure determined at 100K with the p21^{ras}-GppNHp structure determined at 277K [8]. Three of these water molecules might play a key role in the early events of the GTP hydrolysis reaction. A comparison of the p21^{ras}-GppNHp structure re-determined under the same conditions as for the p21^{ras}-GTP structure showed the same shift in the water positions as seen when comparing the GTP structure at 100K with the GppNHp structure at 277K, clearly indicating a dependency on temperature rather than on bound nucleotide. Of further importance is that in the 100K structures, these three water molecules form shorter hydrogen bonds than seen in the 277K structures (Figure 6). In addition, the sidechain of Gln61 is better ordered, forming a hydrogen bond with the attacking water molecule (GppNHp-Wat175). In order to rationalise this observed temperature-dependent positioning, a temperature-dependent change in the dielectric constant and a shrinkage in the occupation-sphere of the individual water molecule might be considered to be important. It might well be, however, that the observed positions have different energy potential functions and therefore different

temperature-dependent occupation. At 100K, only one group of positions is significantly occupied whereas at 277K the other set of positions is predominantly occupied. In GppNHp (100K) for Wat175 only one position is possible, whereas in GTP (100K) for Wat175 there are two positions nearly equal in energy (Wat175-A and Wat175-B). Further experiments with different buffer substances (e.g. the used Tris-HCl buffer has a significant $\Delta pK_a/\Delta T$ value of -0.028 K^{-1}) at different temperatures should give more insight into this phenomenon. If we assume that the 100K water structure is not an artefact but a state that actually occurs on the reaction pathway preceding the situation in which attack occurs, it is possible that the 277K position cannot be seen in the p21^{ras}-GTP structure because a water molecule in this position reacts rapidly. This view implies that the rate-limiting step in the basal GTPase reaction is indeed a process in which, among other things, the attacking water molecule moves closer to the γ -phosphorus.

GppNHp is a good GTP analogue for p21^{ras}

It was suggested some years ago that the rate-limiting step in the cleavage of GTP by p21^{ras} is not the cleavage reaction itself but a conformational change occurring before a rapid hydrolysis step [35,36]. Although this model, or more exactly the hypothesis that GAP must

Figure 6



Scheme of the hydrogen-bond network and metal coordination including distance values around the γ -phosphate group as observed in the p21^{ras}-GTP structure at 100K. For the water molecule Wat175 the two alternative positions (A and B, 1.6 Å apart from each other) are shown. Similarly, for the sidechains of Gln61 and Glu63 the two alternative conformations (A and B) are indicated. In the inset the hydrogen-bonding distances for the water molecules Wat175, Wat189 and Wat190 are given as observed in p21^{ras}-GppNHp (277K) [8].

only accelerate this slow isomerization reaction in order to accelerate the overall hydrolysis reaction, has been challenged and rendered relatively unlikely in its original form by recent evidence on the involvement of an arginine residue from GAP in the chemical mechanism, this does not exclude the possibility that a rate-limiting isomerisation occurs in the basal GTPase reaction. Because the evidence favouring this mechanism is the occurrence of a slow fluorescence change of the p21^{ras}-mant GppNHp complex [36], this would mean that the equilibrium complex between p21^{ras} and GppNHp is an analogue of the p21^{ras}-GTP state immediately after the conformational change and prior to the actual hydrolysis step. In contrast, the p21^{ras}-GTP complex characterised in the present work would, according to this model, be the complex preceding the conformational change. Thus, any differences in the p21^{ras}-GppNHp and p21^{ras}-GTP structure could be interpreted as reflecting this conformational change. We have determined the p21^{ras}-GTP and p21^{ras}-GppNHp structures, respectively, at high-resolution and performed a refinement strategy without geometric restraints for the nucleotide and its environment (see the Materials and methods section). The observed bond lengths and angles together with the values of the estimated standard deviation (esd values) for the phosphate part of the nucleotide are given in the Supplementary material available with the internet version of this paper. The only significant difference is observed for the PB-X-PG bond angle (GTP, $130.4^\circ \pm 2.5^\circ$; GppNHp, $121.8^\circ \pm 1.6^\circ$). Besides this difference, all phosphorus and oxygen atoms are, within the positional error, at identical positions in the different structures.

Insights into the intrinsic hydrolysis mechanism of p21^{ras}

Given that the first structures of p21^{ras} were solved with bound GDP [37] and bound GppNHp [8,38] various models for the hydrolysis mechanism were proposed on the basis of these structures and molecular modelling [8,9]. Site-directed mutagenesis and replacement of Gln61 [6,7] added biochemical data to the understanding of the role of

individual residues. The determination of the relationship between the rate of GTP hydrolysis and the pK_a of the γ -phosphate group [14] was the first experimental indication of the possible role for a 'substrate-assisted catalysis' mechanism [39]. In addition, there is still controversial discussion regarding the basic reaction mechanism, whether it is associative or dissociative [40,41]. In all cases a single water molecule (Wat175, based on the naming in the PDB entry 5P21 [8]) is assumed to be the attacking water molecule. In proposing the γ -phosphate group as the general base [39], it was assumed that there is transfer of a proton from the attacking water molecule itself converting it into a highly nucleophilic hydroxyl ion. We will refer to this as the 'one-water model'.

The work presented here allows a more detailed description of the water structure around the γ -phosphate group at the active site of p21^{ras} before the cleavage reaction occurs. The striking feature is the observation of a concerted shift of three water molecules between different physical states (Figures 5,6) and a well-defined orientation for Gln61 in which the sidechain carbamoyl group forms a hydrogen bond with one of the water molecules, Wat175-A or Wat175-B. The closest water molecule in the 100K structures to any atom of the γ -phosphate group is Wat189, which is now the only one in close hydrogen-bonding distance to phosphate oxygen 3O ($d = 2.6 \text{ \AA}$) and in hydrogen-bonding distance to Wat175-B (Figure 6).

On the basis of these structural observations and the linear free-energy relationship [14], the following flow of events could lead to formation of the transition state for the intrinsic cleavage reaction. First, a proton from Wat189 is donated to the oxygen 3O of the γ -phosphate (the one which is not coordinated to any other protein residue or metal ion in p21^{ras}). This primary protonation step of the phosphate group changes the electrostatic environment and the changed charge distribution and hydrogen-bond network allows Wat175 (the one which is coordinated to Gln61) to move towards the γ -phosphorus atom. After this

shift of ~ 1.5 Å, Wat175 is now in a position in which on the one hand it could form a hydrogen bond to the primary hydroxyl ion and on the other hand is in close contact to the γ -phosphorus atom. In this situation a proton could be exchanged between Wat175 and the primary hydroxy ion resulting in regeneration of Wat189 and formation of a secondary hydroxy ion, this time in close distance to the γ -phosphorus atom. Attack of the approaching water molecule Wat175 or the generated secondary hydroxyl ion could then lead to formation of the transition state. Because in this scenario two water molecules are involved, we will term this flow of events the ‘two-water model’.

If this model is correct, mutants that do not have space for Wat189 should have reduced activity. The structures of three p21^{ras} mutants that introduce a sidechain into this area have been determined in the GTP state or GppNHp state: p21^{ras}(G12D) [21], p21^{ras}(G12V) [26] and p21^{ras}(G12P) [21]. In the first mutant, the aspartic sidechain is oriented close to the positions of Wat189 and forms a direct interaction with the γ -phosphate group and the Gln61 sidechain. Gln61 cannot, therefore, adopt the conformation that would be necessary to position the phosphorus-attacking water molecule (a water molecule at or near the position of Wat175 was not observed [21]). In the last two mutants (solved at 277K), water molecules Wat189 and Wat190 were not observed. Superpositioning and modelling indicates that these water molecules would be too close to any sidechain at residue 12 (Figure 7). Whereas p21^{ras}(G12V) has a dramatically reduced hydrolysis rate ($k_{\text{cat}} = 0.0040 \text{ min}^{-1}$ [7,42,43]), p21^{ras}(G12P) has a slightly faster hydrolysis rate (0.043 min^{-1} [21]) than wild-type p21^{ras}. Proline at position 12 is the only amino acid that can replace glycine and still lead to retention of the intrinsic GTPase activity, which cannot, however, be stimulated by GAP [21,44]. In the course of the present work, we have re-refined the structure of p21^{ras}(G12P)-GppNHp using the same refinement strategy and protocol as for the other structures in order to verify its water structure around the γ -phosphate group. We could not detect a water molecule at or near the positions of Wat189 or Wat190. This might indicate that either the two-water model is not valid or that in the case of p21^{ras}(G12P) another protonation mechanism for the γ -phosphate group can occur. The three mutants share the property that the GTPase reaction cannot be accelerated by GAP. This is most probably because of the important interaction between the carbonyl oxygen of GAP-Arg789 and the sidechain carbamoyl group of p21-Gln61, which is sterically hindered by any sidechain at position 12 of p21^{ras} [45].

Relation to the transition state analogue structures

In order to discuss the relationship of the p21^{ras}-GTP ground state investigated here to the GAP-catalyzed GTPase mechanism (Figures 8a,b), it is necessary to describe briefly the active-site structure of the p21^{ras}-GAP transition state analogue complex published recently (PDB

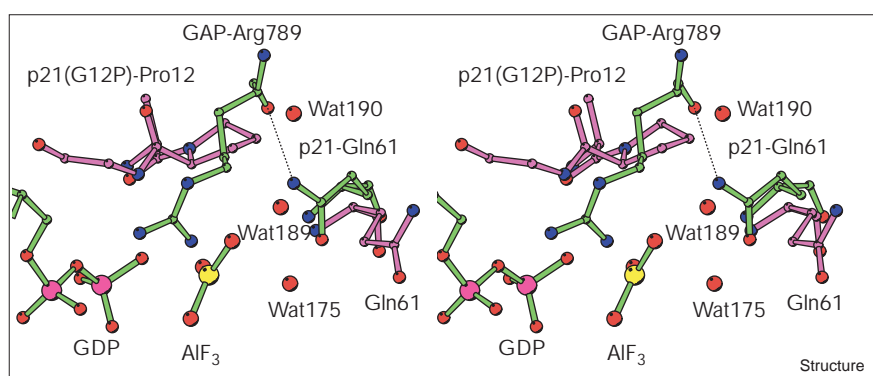
entry 1WQ1 [45]). The description also applies to similar complexes between RhoA and its corresponding GAP [46] (albeit with AlF_4^- instead of AlF_3 in the Scheffzek *et al.* structure [45]) and between Cdc42 and Cdc42GAP [47] in complex with GDP and aluminium fluoride, although the numbering of the amino acid residues differs. In the structure of the complex between p21^{ras}, GAP and aluminium fluoride, the following interactions and structural features are seen (Figure 8b) and, assuming this to be an analogue of the transition state, are concluded provisionally to occur in the actual transition state or a pentavalent phosphorus intermediate in an extreme associative hydrolysis mechanism. We assume that the hydrogen-bonding interactions seen with fluorides are equivalent to interactions with the phosphorus oxygens of the γ -phosphate group in GTP.

The aluminium ion is pentacoordinated, with three equatorial tightly bound (short bond) fluorides and, as axial ligands, a less tightly coordinated oxygen from the β -phosphate of GDP (bond length 2.2 Å) and a water molecule at essentially the same distance. The latter ligand could be either a water molecule interacting through its two hydrogens with both the carbonyl group of Thr35 and with the sidechain of Gln61 or an hydroxy ion with a bifurcated hydrogen bond, in agreement with the geometric requirements [48]. The Gln61 sidechain also interacts with the carbonyl group of Arg789 from GAP, and this interaction must be with the NH_2 group of the glutamine sidechain, which in turn means that its carbonyl group interacts with the water molecule or hydroxy ligand of the aluminium ion. Thus, these interactions, which should also exist in the putative transition state, are with the same groups as found in the GTP ground state described in the present contribution, and we assume by analogy in the ground state it is also the carbonyl group of Gln61, and not the NH_2 , which interacts with the water molecule. This is also in agreement with requirements set by the presence of the hydrogen bond formed between the Gln61 and Glu63 sidechains seen in the 100K structures. A number of other interactions are also seen both in the GTP ground state and in the putative transition state. These are, in particular, the interaction of ^2O of the γ -phosphate with Mg^{2+} and with the backbone NH of Thr35 and the interaction of the sidechain of Lys16 and the backbone NH of Gly60 with ^1O . In the ground state, ^3O does not interact with the protein, although there is an interaction with a water molecule (Wat189), as discussed above.

We can now describe the changes occurring on proceeding from the ground state to the transition state structure as derived from the p21^{ras}-GAP-GDP- AlF_3 structure (and also with equivalent residues in the Rho-RhoGap-GDP- AlF_4^- structure). The only phosphate-protein interactions seen in addition to those in the p21^{ras}-GTP ground state are the interaction of the sidechain NH_1 of GAP-Arg789 with ^3O of the γ -phosphate and with the oxygen bridging the β - and γ -phosphates, and the interaction of the NH_2 group of the

Figure 7

Stereo representation of the p21^{ras}-GDP-AlF₃-GAP structure [45] superimposed with p21^{ras}(G12P)-GppNHp. Displayed residues are Pro12-Gly13 and Gln61 of p21^{ras}(G12P)-GppNHp (in magenta) and GDP, AlF₃ and GAP-Arg789 (in green) of p21^{ras}-GDP-AlF₃-GAP. The water molecules Wat175, Wat189 and Wat190 (red spheres) are placed at the positions where they are seen in the structure of p21^{ras}-GppNHp (277K). The hydrogen bond between the mainchain C = O of GAP-Arg789 and the sidechain group of p21-Gln61 is indicated as a dashed line. This figure was generated using the program Bobscript [59].



sidechain of Gln61 with the same oxygen (that is ³O, Figure 8b). Interestingly, and possibly very importantly, there is now also an interaction of the sidechain of Gln61 with the backbone carbonyl oxygen of GAP-Arg789, as already mentioned. Thus, in comparison with the ground state, it appears that the Gln61-H₂O structure has moved ~2 Å in the direction of the γ-phosphorus, and that this is stabilised by the Gln61-Arg789 and Gln61-³O interaction, whereas the Arg789 sidechain makes an important interaction with ³O of the phosphate group. The role of the arginine residue can be interpreted as stabilising the build up of additional negative charge on the γ-phosphate and indirectly drawing the attacking water molecule nearer to the electrophilic phosphorus by virtue of the mutual interaction with residue Gln61. GAP inserts a further arginine sidechain (Arg903) between Gln61 and Glu63, breaking their hydrogen-bond interaction and therefore enabling the reorientation of the Gln61 sidechain. The role of Gln61 and Thr35 in the ground state appears to be to position the attacking water molecule, which is then brought closer to the γ-phosphate group by GAP although still retaining its interactions with the two residues.

How does this proposed mechanism relate to that discussed above for the basal GTPase (in the absence of GAP)? It is difficult to extend the substrate-assisted principle to the GAP-activated mechanism for the following reasons. If proton transfer to the γ-phosphate from the attacking water occurs, this would presumably be to ³O, because it is not involved in an interaction with the protein in p21^{ras}-GTP. This cannot be reconciled with the evidence that the sidechain of Arg789 from GAP interacts with this oxygen in the transition state with GAP, however, because this requires (or at least is much stronger with) the unprotonated form.

Several points about this scheme should be noted. Firstly, the strong interactions of the protein (p21^{ras}) and Mg²⁺ with the β-phosphate oxygens of GTP and with the β,γ-bridging oxygen withdraw electrons from the β-phosphorus, from

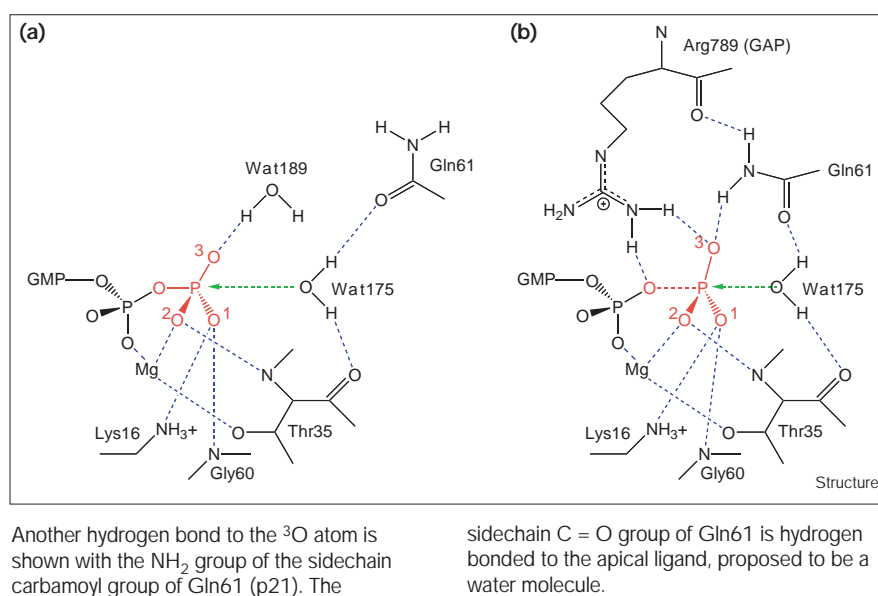
the β,γ-bridging oxygen, and finally from the γ-phosphorus. These effects have been regarded as favouring a dissociative type of mechanism, especially if augmented by further interactions of the β-oxygens with residues from GAP in the transition state, in particular the bridging oxygen [40]. They will also function in a positive catalytic manner in an associative reaction, however, because the electrophilicity of the γ-phosphate is increased, facilitating attack of water or an incipient hydroxyl ion. Thus, interactions with the oxygens of the β-phosphate, both in the ground state and the transition state, could be catalytic for both types of mechanism. Recent Fourier-transform infrared (FTIR) spectroscopy investigations confirm the particularly strong interaction of the β-phosphate with the protein [49].

Secondly, in the model of the transition state derived from the p21^{ras}-GAP-GDP-AlF₃ complex and the corresponding structure with RhoA as well as of the heterotrimeric G proteins, the number of interactions increases significantly, suggesting a mechanism of stabilisation of an associative transition state. In contrast, interactions already present in the ground state would be weakened on formation of a dissociative transition state because of the reduction of total negative charge distributed over the non-bridging oxygens. In a purely dissociative mechanism, the reduction would be from 2 to 1 charges, but even in a mechanism that was only partially dissociative, there would be some loss of charge and consequent weakening of the interactions. This argues strongly against a predominantly dissociative mechanism and the situation becomes even clearer when it is realized that all the interactions seen in the aluminium fluoride structure will be tending to increase the negative charge density on the phosphate oxygens, as expected for an associative mechanism (from 2 to 3 in the extreme case of pure associative with a pentacovalent intermediate).

Thirdly, in general terms, it is difficult to conceive of a mechanism for stabilization of a metaphosphate-like species required by a pure dissociative mechanism. Thus, a dissociative mechanism could be favoured by the factors

Figure 8

Comparison of the protein environment for the intrinsic and GAP-activated GTP hydrolysis of p21^{ras}. (a) Scheme of the proposed ground state of p21^{ras}-GTP for the intrinsic GTP hydrolysis reaction. Wat189 makes two hydrogen bonds, one with the unliganded ³O of the γ -phosphate and the other with Wat175-A (numbering of oxygen atoms in analogy to fluorines in Scheffzek *et al.* [45]). The water molecule Wat175 is held in place by hydrogen bonds with the sidechain carbonyl oxygen of Gln61 and with the mainchain carbonyl oxygen of Thr35. (b) Scheme of the proposed transition state of p21^{ras} in complex with GAP based on the structures of p21^{ras}-GAP-GDP-AlF₃ [45] and Rho-RhoGAP-AlF₄⁻ [46]. No water molecule equivalent to Wat189 is described for this complex. The sidechain guanidinium group of an arginine (GAP residue Arg789) forms one hydrogen bond to the ³O of the γ -phosphate and one to the bridging oxygen between the β -phosphate and γ -phosphate.



mentioned in the first point above, but not by specific interactions with the metaphosphate-like transferred phosphate group in the transition state because the only interactions possible (hydrogen bonds or electrostatic interactions) will tend to stabilise the charge density on the oxygens of the γ -phosphate group and prevent their migration towards the phosphorus and the bridging oxygen to reach the proposed transition state. In a dissociative mechanism, it is to be expected that there would be not only few and weak interactions of the γ -phosphate group with the enzyme in the ground state, but probably destabilising interactions, which could be electrostatic or steric.

Fourthly, interactions with the attacking water molecule, which is the second substrate in the enzymatic reaction, appear to be relatively weak in the ground state, as indicated by the evidence that the presumed catalytically active constellation with interactions of Gln61 and Thr35 is only populated to the extent of ~50%. In the analogue of the transition state, the corresponding interactions appear to be stronger. Thus, they fulfil the expected requirement of being present but relatively weak in the ground state, but strong in the transition state, thus contributing to stabilisation of the transition state relative to the ground state.

Fifthly, a remaining problem in the envisaged mechanism is the fate of the proton of the attacking water molecule, which must be lost at some stage along the reaction coordinate. In a classical associative mechanism, the attacking species would be a hydroxyl ion or an incipient hydroxyl ion. In a dissociative mechanism, the metaphosphate-like species is assumed to be highly reactive, so that even the weakly nucleophilic water molecule would react rapidly with it. Thus, a general base is not considered to be

needed, and the lack of an obvious candidate for this role in the active site of GTPases has been interpreted as evidence against an associative mechanism. This view might be too narrow, however, as the situation is quite different from that in solution, with the γ -phosphate fixed rigidly and a large number of interactions with both the β - and γ -phosphates withdrawing electrons from the γ -phosphorus and rendering it susceptible to nucleophilic attack. In addition to this, the attacking water molecule appears to be positioned by interactions with residues of p21^{ras} and interactions of one of these residues with the catalytic arginine of GAP as the transition state is approached. Presumably, the nucleophilicity of the water molecule is increased by the two hydrogen bonds, even if neither of the groups can be considered to play the role of a general base. We propose therefore, that the attacking species is a water molecule and that in the transition state, a partial bond between the water oxygen and phosphorus is formed. The pK_a value of the water molecule will decrease progressively as the P-O bond is formed, so that at some point along the reaction pathway, dissociation occurs and the pentacovalent intermediate typical of the associative mechanism is formed, or breakage of the bond to the β , γ -bridging oxygen occurs.

Biological implications

GTP-binding proteins cycle between an active GTP-bound state and an inactive GDP-bound state resulting from the hydrolysis of bound GTP to GDP. The present work gives further insights into the local events around the γ -phosphate group of GTP leading to its hydrolysis. We present the possibility that two water molecules are involved in the first events of GTP hydrolysis in the absence of a GTPase-activating protein (GAP), but also propose that in the GAP-mediated hydrolysis reaction

the γ -phosphate of GTP does not become protonated as part of the mechanism. The GTP hydrolysis reaction appears to be predominantly associative in nature. The structures provide further information for understanding the determinants that fine-tune the basal rate of hydrolysis of GTPases of the Ras superfamily, which vary over several orders of magnitude.

For the biological and biophysical characterisation of GTP-binding proteins in their active conformation, slowly-hydrolysable or non-hydrolysable GTP analogues such as GTP γ S and GppNHp are used frequently, but it is possible that these analogues might not truly mimic the GTP-bound state. We have shown that in the case of p21^{ras}, the GTP analogue GppNHp and GTP bind in an identical mode to the protein, albeit with a slightly different positioning of the β,γ -bridging NH group. This is a further justification for using GppNHp as a tool to keep the protein permanently in its active conformation as long as the hydrogen-bonding potential of the bridge is not important. These observations probably also apply to other small GTP-binding proteins of the Ras superfamily.

Materials and methods

Crystallisation

Expression, purification and nucleotide exchange of p21^{ras} (residues 1–166) was performed as described [21]. Crystals were grown in the dark using an established seeding protocol [16]. A protein solution of 25–30 mg/ml p21 (residues 1–166) in 1:1 complex with *R*-caged GTP [18] in 64 mM Tris-HCl (pH 7.6), 10 mM MgCl₂ and 10 mM DTT was mixed with an equal volume of precipitation solution consisting of 56% (v/v) of PEG-400 (Sigma) in 64 mM Tris/HCl (pH 7.6), 10 mM MgCl₂ and 10 mM DTT, incubated for 30 min at 4°C and centrifuged for 30 min at 4°C with 15,000 × g. Drops of 10 μ l were pipetted into a micro batch glass chamber (chamber volume around 500 μ l) seeded with 1 μ l diluted seed solution and sealed with clear sealing tape (Hampton research). Crystals appeared within 10 h and were used for further experiments after 7–10 days. Crystals of p21^{ras}-GppNHp were obtained under the same crystallization conditions, but without the need of seeding. Flash freezing in liquid nitrogen was performed without additional cryoprotectant.

Photolysis of p21^{ras}-caged GTP

The setup for the irradiation of the crystals consisted of a continuous mercury 100 W arc lamp (#6281, LOT Oriol), equipped with a water filter and a UG5 filter. The filtered light was passed through a monochromator (type H10UV, Jobin Yvon - Spex) and the 313 nm \pm 2 nm mercury line was guided with a liquid light fibre (2 mm diameter, Lumatec) into the crystal.

For the preparation of p21^{ras} crystals complexed with GTP a crystal of p21^{ras}-caged GTP with largest dimensions of 200–250 μ m was enriched with fresh DTT (final concentration in the drop \sim 50 mM). The crystal was cooled from 18°C (growth temperature) to 2°C and mounted in its crystallization mother liquor in a nylon loop with a diameter of 300 μ m. To protect the crystal from drying out, the loop was placed in a small plastic cuvette and sealed air-tight. Light of 313 nm was guided with a liquid fibre into the cuvette and focused on the crystal. During irradiation the crystal was rotated to achieve complete illumination from all sides to reduce the inner filter effect. After 2–3 min the conversion of caged GTP to GTP was complete (verified by HPLC analysis of identically treated crystals) and the crystal was shock frozen in liquid nitrogen.

The preparation of p21^{ras} crystals in complex with GDP was based on the same techniques as for p21^{ras}-GTP with a few modifications. The

crystal was not mounted in the loop for irradiation but left in the micro batch crystallisation chamber sealed with clear epoxy tape sitting on a UV mirror. The crystals were kept at growth temperature (18°C). After conversion of caged GTP to GTP the crystal was left in this environment (light switched off) for 6–8 half times of the intrinsic GTP hydrolysis reaction ($T_{1/2}$ is \sim 60 min at this temperature in the crystal) before it was mounted in a nylon fibre loop and shock frozen in liquid nitrogen. The illumination in the batch chamber was necessary because during the incubation for the intrinsic reaction partial drying out of loop-mounted crystals could not be completely avoided.

For all experiments, at least five crystals of the same batch were identically converted into the required nucleotide state. The additional crystals were analyzed by HPLC after shock freezing to serve as controls for photolysis and hydrolysis. The crystal used for data collection was analyzed by HPLC after the collection of diffraction data. For refinement, only those data sets were used where the crystal had a degree of conversion larger than 95% and the nucleotide composition before (HPLC profile of second crystal) and after data collection was not significantly different. Analysis of side reactions induced by photolysis of caged GTP in the presence of DTT that could result in covalent modifications of the protein were performed with electron-spray ionisation mass spectrometry under nanospray conditions [50].

Data collection and processing

Diffraction data for three GTP-, one GppNHp- and two GDP-bound states were collected at 100K (Oxford Cryostream) using a Siemens self rotating copper anode and a Highstar area detector. A third data set of the GDP-bound state at 100K was collected at the HASYLAB beamline BW6 at DESY using a MAR345 image plate detector. A data set of p21^{ras}-GppNHp at 277K was collected at the HASYLAB beamline BW6 at DESY using a MAR-CCD detector. All diffraction frames and images were processed with the program XDS and reduced with the program XSCALE [51]. The individual data sets were obtained from different crystallisation and illumination experiments. The crystals belong to the space group P3₂21, with one complex in the asymmetric unit. A summary of the individual data sets and the processing statistics is given in Table 1.

Refinement

At the beginning of refinement all three GTP and GDP structures were processed and refined independently. Starting phases were calculated using the p21^{ras}-GppNHp(277K) structure (PDB entry 5P21 [8]) without nucleotide, magnesium ion, water molecules and the loop regions from residues 30–38 and 60–68. The initial refinement was carried out using the programs X-PLOR and CNS, respectively [25,52–54] and the CCP4 program package [55]. The different structures were refined in parallel using identical refinement strategies. Display of electron-density maps, interpretation and subsequent model building was carried out with O [56]. Because the most important aspect for the presented work were the surroundings of the γ -phosphate group, the sidechains for residues 61–68 and the coordinated water molecules were built last after no further significant $F_{\text{obs}}-F_{\text{calc}}$ difference electron-density peaks showed up for the remaining parts of the molecule. After the refinement of the individual data sets had converged, a first comparison of the individual structures was performed to identify deviations from one experiment to the other. These comparisons were based on the interpretation of simulated annealing omit maps, σ_a -weighted $2F_{\text{obs}}-F_{\text{calc}}$ and of $F_{\text{obs}}-F_{\text{obs}}$ electron-density maps, respectively. Because in all three structures the same alternative conformations for sidechains (residues Asn26, Thr50, Thr74 and Cys118) and no significant differences around the γ -phosphate group could be observed, an averaged and normalised electron-density map was calculated in real space from the individual electron-density maps (using the program 4d_mapman [57]). These maps showed significantly reduced noise compared with the individual electron-density maps. For further refinement the three individual data sets were scaled together (XSCALE) to obtain one high-quality data set. To be able to calculate estimated standard deviations (esd) for individual atom positions, bond lengths and bond angles, further

Table 1

Data collection, processing and model refinement statistics for p21^{ras}-GTP, p21^{ras}-GppNHp and p21^{ras}-GDP.

	p21 ^{ras} -GTP			p21 ^{ras} -GppNHp		p21 ^{ras} -GDP*	
	T1	T2	T3	T1 + T2 + T3	N1	N2	D1
Data statistics							
Temperature (K)	100	100	100		100	277	100
Resolution limit (Å)	1.86	1.6	1.5		1.25	1.3	1.9
Cell dimensions (P3 ₂ 21)	a = b = 39.6; c = 159.3.1	a = b = 39.6; c = 159.3	a = b = 39.6; c = 159.4		a = b = 39.6; c = 158.4	a = b = 40.1; c = 160.4	a = b = 39.7; c = 154.1
Average redundancy	2.8	6.1	3	9.1	3	4	2.8
R _{merge} (%) [†]	3.3	4.1	3.2	6.9	2.7	8.3	8.0
Refinement statistics							
Resolution limit (Å)	1.9	1.7	1.6	1.6	1.25	1.35	2.0
Completeness of data (%)	77.1 [35.6] [§]	95.9 [91.3] [§]	96.5 [74.5] [§]	99.8 [87.1] [§]	86.3 [58.8] [§]	87.4 [66.1] [§]	87.3 [77] [§]
R _{cryst} (%) / (R _{free} (%) [#]) [¶]	20.2/23.4	19.0/21.9	19.6/22.9	16.8/23.0	17.1/22.2	21.9/24.3	26.5/31.6 [†]
Rms bond lengths (Å)	0.007	0.007	0.01	0.008	0.010	0.009	0.007
Rms bond angles (°)	1.404	1.408	1.475	1.480	2.29	1.402	1.264
No. of water molecules	114	154	168	232	256	160	64
Mean/rms on B factors (Å ²)							
overall	26.2/13.2	20.1/10.5	20.4/12.2	23.9/13.4	17.5/11.8	24.5/10.7	32.3/13.8
nucleotide + Mg(II)	20.2/2.7	13.6/1.4	12.5/1.6	13.7/1.5	8.6/1.4	15.0/1.8	25.6/5.5
solvent	32.0/8.7	32.2/12.2	34.6/13.7	40.3/15.6	31.5/14.0	42.7/12.7	36.3/11.3

*The refinement for three independent crystal structures of p21^{ras}-GDP are in progress; the statistics of the best data set are given for the comparison (see Results section). [†]The high-resolution data were collected at beamline BW6 (DESY-HASYLAB, Hamburg) using a Mar345 imaging plate and combined with a low-resolution (100–1.5 Å) data set collected in-house. [‡]R_{merge} = 100 × Σ|I_o - <I>| / ΣI, where I is the observed intensity and <I> is the average intensity calculated from multiple

observations of symmetry-related reflections. [§]In square brackets are quantities calculated in the highest resolution shell used for refinement: 2.0–1.9, 1.8–1.7, 1.7–1.6 and 1.7–1.6 Å for data columns T1, T2, T3 and T1 + T2 + T3, respectively. [#]R_{cryst} = 100 × Σ|F_o - F_c| / Σ|F_o|, where F_o and F_c are observed and calculated amplitudes, respectively. [¶]R_{free} is an R_{cryst} calculated using 5% of the processed data, chosen randomly, kept constant and omitted from all subsequent structure refinement steps [53].

refinement against F²-values was carried out using [23] keeping the same set of reflections for R_{free} cross-validation. Conjugate gradient least-squares (CGLS) cycles (10) were performed in each of five consecutive SHELXL refinement jobs, global restraint esd defaults (DEFS) were set to 0.02 0.1 0.01 0.04, refinement of diffuse solvent parameter (SWAT) and anisotropic scaling (HOPE) were included step-wise. Only the magnesium ion and the sulfur and phosphorus atoms were refined anisotropically in the last CGLS refinement run. After each refinement the complete model was checked based on σ_a-weighted electron-density maps. After convergence using conjugate-gradient least-squares (CGLS) refinement one cycle of full-matrix least-squares refinement (LS) was performed with all restraints switched off. Calculation of bond lengths, angles and connected esd values was performed with the RTAB option.

Accession numbers

Coordinates of p21^{ras}-GTP and p21^{ras}-GppNHp (100K) have been deposited in the Protein Data Bank with entry codes 1QRA and 1CTQ, respectively [58].

Supplementary material

Supplementary material including figures describing the detailed bond lengths and angles of the nucleotides and a more detailed table of structure statistics is available at <http://current-biology.com/supmat/supmatin.htm>.

Acknowledgements

We thank John E Corrie and Gordon Reid for pure diastereoisomers of caged GTP, Karin Illner for protein purification, Igor Chizhov for technical advice regarding flash-photolysis, Ingrid Vetter, Arnon Lavie and Georg Holtermann for assistance with data collection, Heino Prinz for mass spectrometry, Thomas Schneider for very useful discussions during structure refinement and providing an extra large version of SHELXL, and Ilme

Schlichting for valuable discussions throughout the course of this work. This research was funded by the BMB+F.

References

- Bourne, H.R., Sanders, D.A. & McCormick, F. (1990). The GTPase superfamily: a conserved switch for diverse cell functions. *Nature* **348**, 125-131.
- Kjeldgaard, M., Nyborg, J. & Clark, B.F. (1996). The GTP binding motif: variations on a theme. *FASEB J.* **10**, 1347-1368.
- Sprang, S.R. (1997). G protein mechanisms - insights from structural analysis. *Annu. Rev. Biochem.* **66**, 639-678.
- Wittinghofer, A., Scheffzek, K. & Ahmadian, M.R. (1997). The interaction of Ras with GTPase-activating proteins. *FEBS Lett.* **410**, 63-67.
- Feuerstein, J., Goody, R.S. & Webb, M.R. (1989). The mechanism of guanosine nucleotide hydrolysis by p21 c-Ha-ras: The stereochemical course of the GTPase reaction. *J. Biol. Chem.* **264**, 6188-6190.
- Chung, H.H., Benson, D.R., Cornish, V.W. & Schultz, P.G. (1993). Probing the role of loop 2 in Ras function with unnatural amino acids. *Proc. Natl Acad. Sci. USA* **90**, 10145-10149.
- Frech, M., *et al.*, & Wittinghofer, A. (1994). Role of glutamine-61 in the hydrolysis of GTP by p21H-ras: an experimental and theoretical study. *Biochemistry* **33**, 3237-3244.
- Pai, E.F., Krengel, U., Petsko, G.A., Goody, R.S., Kabsch, W. & Wittinghofer, A. (1990). Refined crystal structure of the triphosphate conformation of H-ras p21 at 1.35 Å resolution: implications for the mechanism of GTP hydrolysis. *EMBO J.* **9**, 2351-2359.
- Privé, G.G., *et al.*, & Kim, S.H. (1992). X-ray crystal structures of transforming p21 ras mutants suggest a transition-state stabilization mechanism for GTP hydrolysis. *Proc. Natl Acad. Sci. USA* **89**, 3649-3653.
- Kraulis, P.J., Dommelle, P.J., Campbell-Burk, S.L., Van Aken, T. & Laue, E.D. (1994). Solution structure and dynamics of ras p21.GDP determined by heteronuclear three- and four-dimensional NMR spectroscopy. *Biochemistry* **33**, 3515-3531.
- Ito, Y., *et al.*, & Miyazawa, T. (1997). Regional polyserism in the GTP-bound form of the human c-Ha-Ras protein. *Biochemistry* **36**, 9109-9119.

12. Ma, J.P. & Karplus, M. (1997). Ligand-induced conformational changes in ras p21 - a normal mode and energy minimization analysis. *J. Mol. Biol.* **274**, 114-131.
13. Diaz, J.F., Wroblowski, B., Schlitter, J. & Engelborghs, Y. (1997). Calculation of pathways for the conformational transition between the GTP- and GDP-bound states of the Ha-ras-p21 protein: calculations with explicit solvent simulations and comparison with calculations in vacuum. *Proteins* **28**, 434-451.
14. Schweins, T., Geyer, M., Scheffzek, K., Warshel, A., Kalbitzer, H.R. & Wittinghofer, A. (1995). Substrate-assisted catalysis as a mechanism for GTP hydrolysis of p21ras and other GTP-binding proteins. *Nat. Struct. Biol.* **2**, 36-44.
15. Schlichting, I., Rapp, G., John, J., Wittinghofer, A., Pai, E.F. & Goody, R.S. (1989). Biochemical and crystallographic characterization of a complex of c-Ha-ras p21 and caged GTP with flash photolysis. *Proc. Natl Acad. Sci. USA* **86**, 7687-7690.
16. Scheidig, A.J., et al., & Goody, R.S. (1994). Crystallographic studies on p21H-ras using the synchrotron Laue method: improvement of crystal quality and monitoring of the GTPase reaction at different time points. *Acta Crystallogr. D* **50**, 512-520.
17. Cherfils, J., Menetrey, J., Le Bras, G., Janoueix-Lerosey, I., de Gunzburg, J., Garel, J.R. & Auzat, I. (1997). Crystal structures of the small G protein Rap2A in complex with its substrate GTP, with GDP and with GTPγS. *EMBO J.* **16**, 5582-5591.
18. Scheidig, A.J., et al., & Goody, R.S. (1995). X-ray crystal structure analysis of the catalytic domain of the oncogene product p21H-ras complexed with caged GTP and MANT dGppNHP. *J. Mol. Biol.* **253**, 132-150.
19. Walker, J.W., Reid, G.P., McCray, J.A. & Trentham, D.R. (1988). Photolabile 1-(2-nitrophenyl)ethyl phosphate esters of adenine nucleotide analogues. Synthesis and mechanism of photolysis. *J. Am. Chem. Soc.* **110**, 7170-7177.
20. Rapp, G. (1998). Flash-lamp based irradiation of caged-compounds. In *Methods in Enzymology* (Marriott G., ed.), Academic Press, New York, **291**, 202-222.
21. Franken, S.M., et al., & Wittinghofer, A. (1993). Three-dimensional structures and properties of a transforming and a nontransforming glycine-12 mutant of p21H-ras. *Biochemistry* **32**, 8411-8420.
22. Rensland, H., et al., & Goody, R.S. (1995). Substrate and product structural requirements for binding of nucleotides to H-ras p21: the mechanism of discrimination between guanosine and adenosine nucleotides. *Biochemistry* **34**, 593-599.
23. Sheldrick, G.M. & Schneider, T.R. (1997). SHELXL: High resolution refinement. In *Methods in Enzymology* (Carter C.W. Jr. & Sweet R.M., eds.), **277**, pp. 319-343, Academic Press, New York.
24. Abagyan, R.A., Totrov, M.M. & Kuznetsov, D.N. (1994). ICM - a new method for protein modeling and design. Applications to docking and structure prediction from the distorted native conformation. *J. Comp. Chem.* **15**, 488-506.
25. Brünger, A.T., et al., & Warren, G.L. (1998). Crystallography and NMR system - a new software suite for macromolecular structure determination. *Acta Crystallogr. D* **54**, 905-921.
26. Schlichting, I., et al., & Goody, R.S. (1990). Time-resolved X-ray crystallographic study of the conformational change in Ha-Ras p21 protein on GTP hydrolysis. *Nature* **345**, 309-315.
27. Milburn, M.V., et al., & Kim, S.H. (1990). Molecular switch for signal transduction: structural differences between active and inactive forms of protooncogenic ras proteins. *Science* **247**, 939-945.
28. Berchtold, H., Reshetnikova, L., Reiser, C.O., Schirmer, N.K., Sprinzl, M. & Hilgenfeld, R. (1993). Crystal structure of active elongation factor Tu reveals major domain rearrangements. *Nature* **365**, 126-132.
29. Kjeldgaard, M., Nissen, P., Thirup, S. & Nyborg, J. (1993). The crystal structure of elongation factor EF-Tu from *Thermus aquaticus* in the GTP conformation. *Structure* **1**, 35-50.
30. Noel, J.P., Hamm, H.E. & Sigler, P.B. (1993). The 2.2 Å crystal structure of transducin-α complexed with GTPγS. *Nature* **366**, 654-663.
31. Sydor, J.R., Engelhard, M., Wittinghofer, A., Goody, R.S. & Herrmann, C. (1998). Transient kinetic studies on the interaction of Ras and the Ras-binding domain of c-Raf-1 reveal rapid equilibration of the complex. *Biochemistry* **37**, 14292-14299.
32. Stouten, P.F.W., Sander, C., Wittinghofer, A. & Valencia, A. (1993). How does the switch II region of G-domains work? *FEBS Lett.* **320**, 1-6.
33. Garman, E.F. & Schneider, T.R. (1998). Macromolecular cryocrystallography. *J. Appl. Crystallogr.* **30**, 211-237.
34. Rodgers, D.W. (1997). Practical cryocrystallography. In *Methods in Enzymology* (Carter C.W. Jr. & Sweet R.M., eds.), Academic Press, New York, **276**, 183-203.
35. Moore, K.J., Webb, M.R. & Eccleston, J.F. (1993). Mechanism of GTP hydrolysis by p21N-ras catalyzed by GAP: studies with a fluorescent GTP analogue. *Biochemistry* **32**, 7451-7459.
36. Neal, S.E., Eccleston, J.F. & Webb, M.R. (1990). Hydrolysis of GTP by p21NRAS, the NRAS protooncogene product, is accompanied by a conformational change in the wild-type protein: use of a single fluorescent probe at the catalytic site. *Proc. Natl Acad. Sci. USA* **87**, 3562-3565.
37. Tong, L., de Vos, A.M., Milburn, M.V. & Kim, S.H. (1991). Crystal structures at 2.2 Å resolution of the catalytic domains of normal ras protein and an oncogenic mutant complexed with GDP. *J. Mol. Biol.* **217**, 503-516.
38. Pai, E.F., Kabsch, W., Krengel, U., Holmes, K.C., John, J. & Wittinghofer, A. (1989). Structure of the guanine-nucleotide-binding domain of the Ha-ras oncogene product p21 in the triphosphate conformation. *Nature* **341**, 209-214.
39. Schweins, T. & Warshel, A. (1996). Mechanistic analysis of the observed linear free energy relationships in p21ras and related systems. *Biochemistry* **35**, 14232-14243.
40. Maegley, K.A., Admiraal, S.J. & Herschlag, D. (1996). Ras-catalyzed hydrolysis of GTP: a new perspective from model studies. *Proc. Natl Acad. Sci. USA* **93**, 8160-8166.
41. Mildvan, A.S. (1997). Mechanisms of signaling and related enzymes. *Proteins* **29**, 401-416.
42. Gideon, P., et al., & Wittinghofer, A. (1992). Mutational and kinetic analyses of the GTPase-activating protein (GAP)-p21 interaction: the C-terminal domain of GAP is not sufficient for full activity. *Methods Mol. Biol.* **12**, 2050-2056.
43. Farnsworth, C.L., Marshall, M.S., Gibbs, J.B., Stacey, D.W. & Feig, L.A. (1991). Preferential inhibition of the oncogenic form of RasH by mutations in the GAP binding/effector domain. *Cell* **64**, 625-633.
44. Seeburg, P.H., Colby, W.W., Capon, D.J., Goeddel, D.V. & Levinson, A.D. (1984). Biological properties of human c-Ha-ras1 genes mutated at codon 12. *Nature* **312**, 71-75.
45. Scheffzek, K., et al., & Wittinghofer, A. (1997). The Ras-RasGAP complex: structural basis for GTPase activation and its loss in oncogenic Ras mutants. *Science* **277**, 333-338.
46. Rittinger, K., Walker, P.A., Eccleston, J.F., Smerdon, S.J. & Gamblin, S.J. (1997). Structure at 1.65 Å of RhoA and its GTPase-activating protein in complex with a transition-state analogue. *Nature* **389**, 758-762.
47. Nassar, N., Hoffman, G.R., Manor, D., Clardy, J.C. & Cerione, R.A. (1998). Structures of Cdc42 bound to the active and catalytically compromised forms of Cdc42GAP. *Nat. Struct. Biol.* **5**, 1047-1052.
48. Jeffrey, G.A. & Maluszynska, H. (1990). The stereochemistry of the water molecules in the hydrates of small biological molecules. *Acta Crystallogr. B* **46**, 546-549.
49. Cepus, V., Scheidig, A.J., Goody, R.S. & Gerwert, K. (1998). Time-resolved FTIR studies of the GTPase reaction of H-ras p21 reveal a key role for the beta-phosphate. *Biochemistry* **37**, 10263-10271.
50. Wilim, M., et al., & Mann, M. (1996). Femtomole sequencing of proteins from polyacrylamide gels by nano-electrospray mass spectrometry. *Nature* **379**, 466-469.
51. Kabsch, W. (1993). Automatic processing of rotation diffraction data from crystals of initially unknown symmetry and cell constants. *J. Appl. Crystallogr.* **26**, 795-800.
52. Brünger, A.T., Kuriyan, J. & Karplus, M. (1987). Crystallographic R-factor refinement by molecular dynamics. *Science* **235**, 458-460.
53. Brünger, A.T., Krukowski, A. & Erickson, J.W. (1990). Slow cooling protocols for crystallographic refinement by simulated annealing. *Acta Crystallogr. A* **46**, 583-593.
54. Brünger, A.T. (1992). Free R value: a novel statistical quantity for assessing the accuracy of crystal structures. *Nature* **355**, 472-475.
55. CCP4 (1994). The CCP4 suite: Programs for protein crystallography. *Acta Crystallogr. D* **50**, 760-763.
56. Jones, T.A., Zou, J.Y., Cowan, S.W. & Kjeldgaard, M. (1991). Improved methods for binding protein models in electron-density maps and the location of errors in these models. *Acta Crystallogr. A* **47**, 110-119.
57. Kleywegt, G.J. & Jones, T.A. (1996). *xd1MAPMAN* and *xd1DATAMAN* - programs for reformating, analysis and manipulation of biomacromolecular electron-density maps and reflection data sets. *Acta Crystallogr. D* **52**, 826-828.
58. Bernstein, F.C., et al., & Tasumi, M. (1977). The protein data bank: a computer-based archival file for macromolecular structures. *J. Mol. Biol.* **112**, 535-542.
59. Esnouf, R.M. (1997). An extensively modified version of MolScript that includes greatly enhanced coloring capabilities. *J. Mol. Graph.* **15**, 133-138.

The pre-hydrolysis state of p21^{ras} in complex with GTP: new insights into the role of water molecules in the GTP hydrolysis reaction of ras-like proteins

Axel J Scheidig, Christoph Burmester and Roger S Goody

Structure November 1999, 7:1311–1324

Table S1

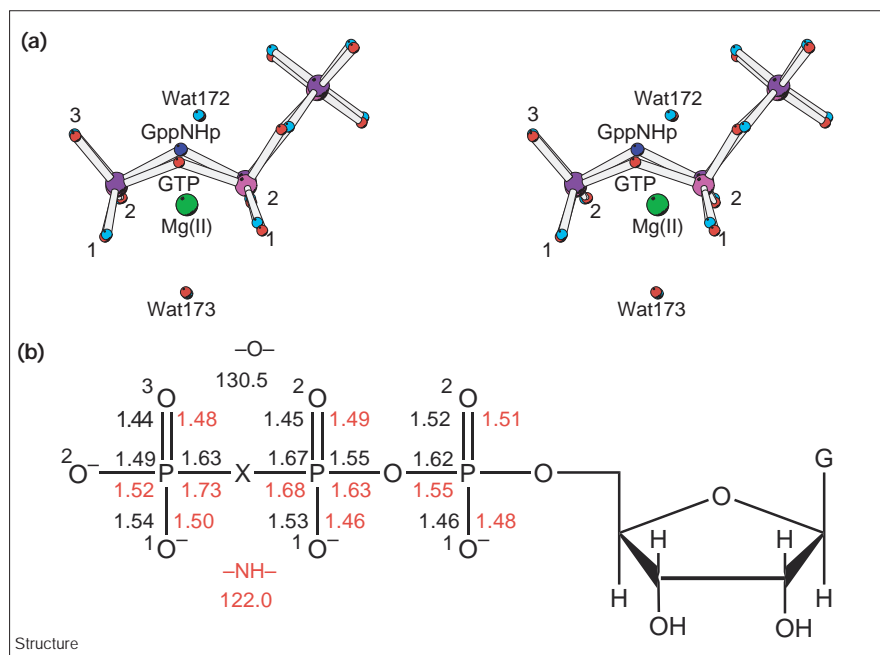
Data collection, processing and model refinement statistics for p21^{ras}-GTP, p21^{ras}-GppNHP and p21^{ras}-GDP.

	p21 ^{ras} -GTP				p21 ^{ras} -GppNHP		p21 ^{ras} -GDP*
	T1	T2	T3	T1 + T2 + T3	N1	N2	D1
Data statistics							
Area detector	HiStar	HiStar	HiStar		HiStar	Mar345/Histar ⁸	HiStar
Wavelength (Å)	1.54	1.54	1.54		1.54	1.0/1.54	1.54
Temperature (K)	100	100	100		100	277	100
Resolution limit (Å)	1.86	1.6	1.5		1.25	1.3	1.9
Cell dimensions (P3 ₂ 21)	a = b = 39.6; c = 159.3.1	a = b = 39.6; c = 159.3	a = b = 39.6; c = 159.4		a = b = 39.6; c = 158.4	a = b = 40.1; c = 160.4	a = b = 39.7; c = 154.1
No. of observed reflections	28,185	11,4822	63,687		105,982	124,045	28,586
Average redundancy	2.8	6.1	3	9.1	3	4	2.8
R _{merge} (%) [†]	3.3	4.1	3.2	6.9	2.7	8.3	8.0
Intensities <I/σ>	21.1 [4.1] [§]	22.2 [3.2] [§]	21.0 [4.5] [§]	30.7 [5.0] [§]	28.9 [6.7] [§]	9.24 [2.45] [§]	17.7 [3.4] [§]
Structure factors <F/σ>	42.1 [7.9] [§]	44.2 [6.2] [§]	41.9 [9.7] [§]	61.3 [9.9] [§]	57.9 [13.1] [§]	18.3 [4.8] [§]	35.4 [7.9] [§]
Refinement statistics							
Resolution limit (Å)	1.9	1.7	1.6	1.6	1.25	1.35	2.0
No. of unique reflections	9356	16,158	19,311	21,641	35,100	29,807	8915
Completeness of data (%)	77.1 [35.6] [#]	95.9 [91.3] [#]	96.5 [74.5] [#]	99.8 [87.1] [#]	86.3 [58.8] [#]	87.4 [66.1] [#]	87.3 [77] [#]
R _{cryst} (%) / (R _{free} (%) [‡])	20.2/23.4	19.0/21.9	19.6/22.9	16.8/23.0	17.1/22.2	21.9/24.3	26.5/31.6 [†]
Rms bond lengths (Å)	0.007	0.007	0.01	0.008	0.010	0.009	0.007
Rms bond angles (°)	1.404	1.408	1.475	1.480	2.29	1.402	1.264
Rms Δω (°) ^{**}	1.3	1.5	1.6	5.5	5.6	1.6	1.2
No. of nonhydrogen atoms	1469	1509	1523	1649	1668	1629	1411
No. of water molecules	114	154	168	232	256	160	64
Mean/rms on B factors (Å ²)							
overall	26.2/13.2	20.1/10.5	20.4/12.2	23.9/13.4	17.5/11.8	24.5/10.7	32.3/13.8
backbone	23.0/10.6	16.7/7.9	16.2/8.5	18.5/8.6	17.6/11.1	21.1/8.4	30.9/12.5
sidechain	28.7/15.5	20.9/10.4	21.5/12.2	24.5/12.3	18.0/11.1	24.3/7.9	33.7/15.3
nucleotide + Mg(II)	20.2/2.7	13.6/1.4	12.5/1.6	13.7/1.5	8.6/1.4	15.0/1.8	25.6/5.5
solvent	32.0/8.7	32.2/12.2	34.6/13.7	40.3/15.6	31.5/14.0	42.7/12.7	36.3/11.3

*The refinement for three independent crystal structures of p21^{ras}-GDP are in progress; the statistics of the best data set are given for the comparison (see Results section). [†]The high-resolution data were collected at beamline BW6 (DESY-Hasylab, Hamburg) using a Mar345 imaging plate and combined with a low-resolution (100–1.5 Å) data set collected in house. [‡]R_{merge} = 100 × Σ|I - <I>| / ΣI, where I is the observed intensity and <I> is the average intensity calculated from multiple observations of symmetry-related reflections. [§]In square brackets are quantities calculated in the highest resolution shell collected: 2.0–1.86, 1.8–1.6, 1.7–1.54, 1.7–1.54, 1.35–1.25,

1.4–1.3 and 1.9–2.0 Å for data columns T1, T2, T3, T1 + T2 + T3, N1, N2 and D1, respectively. [#]In square brackets are quantities calculated in the highest resolution shell used for refinement: 2.0–1.9, 1.8–1.7, 1.7–1.6 and 1.7–1.6 Å for data columns T1, T2, T3 and T1 + T2 + T3, respectively. [†]R_{cryst} = 100 × Σ|F_o - F_c| / Σ|F_o|, where F_o and F_c are observed and calculated amplitudes, respectively. [‡]R_{free} is an R_{cryst} calculated using 5% of the processed data, chosen randomly, kept constant and omitted from all subsequent structure refinement steps [53]. ^{**}Δω is the deviation of the peptide torsion angle from 180°.

Figure S1



Comparison of the bond lengths and angles in the phosphate part of GTP and GppNHp. (a) The triphosphate chain is superimposed together with the Mg^{2+} ion and its coordinating water molecules. (b) Bond lengths and the angle at the β,γ -bridging heteroatom (X = O in GTP and X = NH in GppNHp). The values were calculated in SHELXL with the RTAB option after a least-squares refinement without any restraints (numbers in red are for GppNHp). The mean estimated standard deviation (esd) is 0.04 Å (bonds) and 2.5° (angles) for GTP and 0.025 Å (bonds) and 1.5° (angles) for GppNHp. This figure was generated using Bobscript [59].